10 Particle physics with CMS

E. Aguiló, E. Alagöz[2], C. Amsler, S. de Visscher, M. Ivova, B. Millán Mejías, P. Otyugova, C. Regenfus, P. Robmann, J. Rochet, T. Rommerskirchen, A. Schmidt, S. Steiner, D. Tsirigkas[3], and L. Wilke[4]

V. Chiochia, C. Favaro, A. Jaeger, and H. Snoek

In collaboration with: Paul Scherrer Institut (PSI) and the CMS Collaboration

The silicon pixel detector is the innermost component of the CMS experiment (1) at the LHC. It allows a precise reconstruction of the directions of charged particles and the identification of displaced vertices from long-lived particle decays. The 53 cm long barrel pixel section, counting about 48 million channels, consists of three cylindrical layers at radii between 4.4 cm and 10.2 cm. Two endcap disks at each side of the barrel provide coverage up to large rapidities.

We were involved since 1995 in the design, construction and commissioning of the barrel pixel detector (1). We have led prototype tests with CERN beams, measuring sensor performances before and after irradiation, such as position resolution, detection efficiency, charge sharing and Lorentz deflection. In addition, we have contributed to the development and commissioning of the readout chip. We have designed and built in the Institute workshop the mechanical and cooling structure and the two service tubes which provide coolant and power, and transfer the signals to and from the pixel detector. Details can be found in earlier reports and in various publications such as refs. (2; 3; 4).

After a commissioning phase with cosmic rays CMS started recording proton collisions in December 2009 at the center-of-mass energy of 900 GeV (Fig. 10.1). During the run a world record center-of-mass energy of 2.36 TeV was achieved with the LHC. A first physics publication on multiplicity distributions has already appeared (5). A run at 7 TeV has started in March 2010 (Fig. 10.2) which is expected to last until autumn 2011, with the goal to reach an integrated luminosity of 1 fb^{-1}.

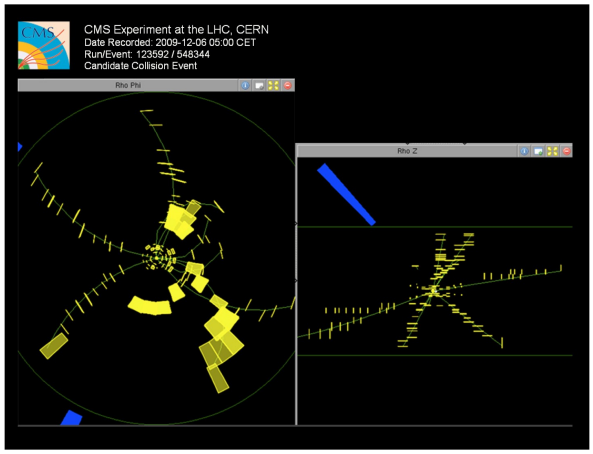

Figure 10.1: Event displays of the first pp-collisions registered by CMS at 900 GeV in December 2009.

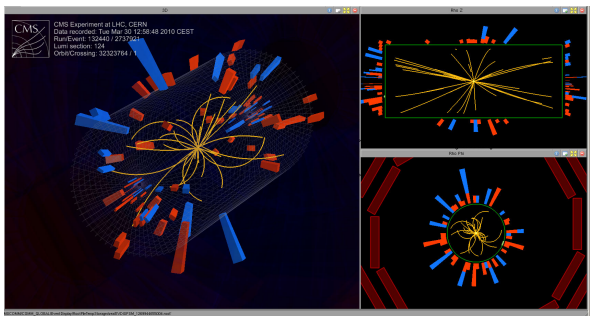

Figure 10.2: Event displays of pp-collisions at 7 TeV registered in March 2010.

[2]until 31 August 2009.
[3]until 31 August 2009.
[4]until 31 December 2009.

10.1 Commissioning of CMS silicon pixel detector with first collision data

As the CMS pixel detector plays a key role for several physics analyses, our first priority was to measure its performance with LHC collisions and to compare with expectations. Last year we performed several important measurements and calibrations, ranging from a measurement of the detector occupancy and position resolution to that of the Lorentz angle in the 3.8 T magnetic field.

First, background events such as beam-halo or beam-gas interactions have to be carefully removed during the offline selection. We have developed several rejection algorithms that are now employed in CMS analyses and have studied the dependence of the background rate on LHC operating conditions. In the near future we will also test the effects of beam tuning on the background rate.

One of the most important benchmarks is the occupancy which provides estimates of the detector noise. The comparison with expectations from event generators is also very important to fine-tune phenomenological parameters such as parton showers and multiple partons interaction, which influence charged particle production at very low momenta, and can produce a large number of hits in the innermost layers of the pixel detector. The pixel detector occupancy was measured at 0.9 TeV and 2.36 TeV center-of-mass energies for the barrel section (see Fig. 10.3), and for single barrel modules (or blades in the endcap sections). The average occupancy is in very good agreement with expectations, with discrepancies generally smaller than 5%. However, fine tuning of the Monte Carlo generators will be needed as no fitting to data was attempted so far for LHC energies.

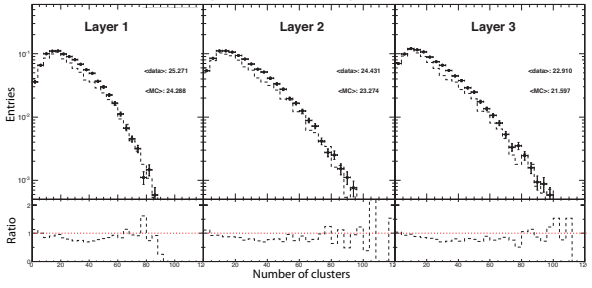

Figure 10.3: Measured (dots) and simulated pixel hit multiplicities in the three barrel layers at 900 GeV. The bottom plots show the ratios between measurements and simulations.

Charge collection was also compared to Monte Carlo simulation (Fig. 10.4). The pixel cluster charges were normalized to the path lengths in the silicon sensors. We observed excellent agreement with simulation for the peak position, width and tails of the distribution, hence have a very good understanding of the analogue readout chain and charge calibration.

A measurement of the position resolution was performed using first collision data. We used pairs of consecutive hits along trajectories in the overlap regions between adjacent modules of a given layer, and calculated the differences in hit positions Δx_{hit} (Δy_{hit}) along the transverse (longitudinal) direction. We then

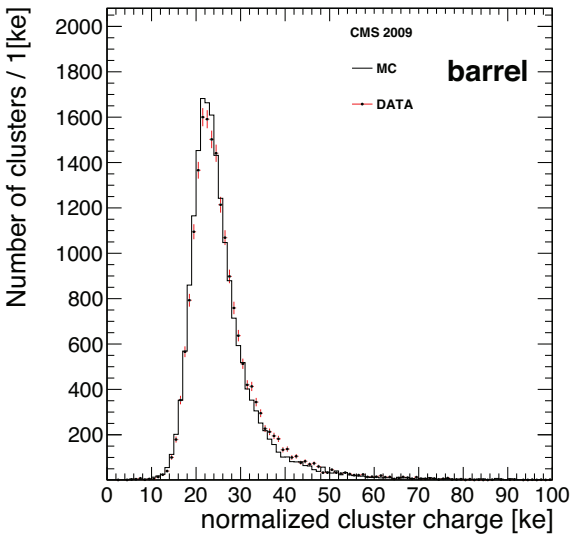

Figure 10.4: Measured (dots) and simulated cluster charge distribution in the barrel pixel detector.

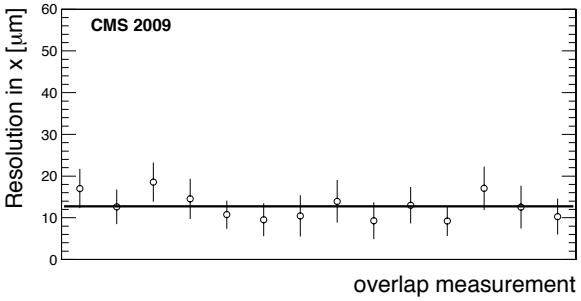

Figure 10.5: Position resolution for the barrel detector along the transverse coordinates. Each point corresponds to a pair of overlapping modules, calculated from more than 20 crossing tracks. The solid line shows the average resolution.

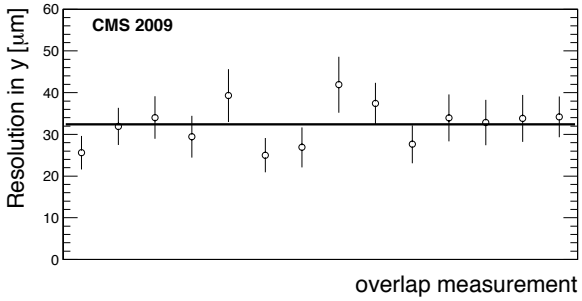

Figure 10.6: As in Fig. 10.5 but along the longitudinal coordinates.

computed the double difference, Δx (Δy) between Δx_{hit} (Δy_{hit}) and the differences Δx_{pred} (Δy_{pred}) between the expected positions from trajectory extrapolation. The double difference distribution was then fitted with a Gaussian and the uncertainty on the predicted position quadratically subtracted from the width, to recover the intrinsic hit resolution. The results are shown in Figs. 10.5 and 10.6. Each point represents the resolution measurement for a different pair of overlapping modules. The mean value is shown as a solid line in the plot. The r.m.s. resolutions are 12.9±3.0 μm along the transverse coordinate (x) and 32.4±4.9 μm along the longitudinal coordinate (y). The same technique on a Monte Carlo sample gives results in agreement with data.

Ionization charges produced by particles traversing the pixel sensors drift under the combined electric and magnetic fields. The ensuing Lorentz angle between drift direction and electric field leads to a systematic shift of the hit position that has to be corrected. The shift depends on various experimental conditions such as bias voltage, temperature and irradiation, and has therefore to be measured in-situ and monitored. Measurements of the Lorentz angle with the barrel pixel detector were performed with the 2009 cosmic ray run (CRAFT09 (6)). Since detector operating conditions (bias voltage, temperature, etc.) were different from the 2008 data (CRAFT08), a different Lorentz angle was expected (7; 8). The angle was measured by finding the minimum of the mean cluster size distribution, measured as a function of the track incidence angle (9). The result (first row in Table 10.1) is in good agreement with the prediction from the PIXELAV simulation (10). As expected, the measured value (Fig. 10.7) was about 2° lower than for CRAFT08.

The measurements were repeated with tracks from proton collisions using the "grazing angle" technique (11). The transverse cluster dis-

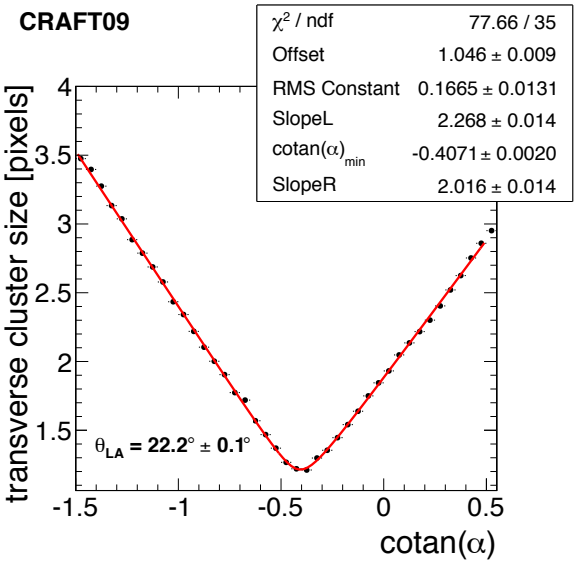

Figure 10.7: Measurements of the Lorentz angle in the 3.8 T magnetic field: pixel cluster size as a function of incidence angle from cosmic rays.

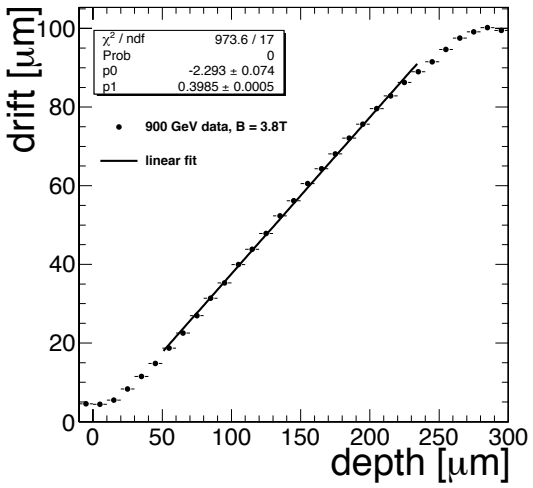

Figure 10.8: Transverse cluster displacement as a function of sensor depth for minimum bias events.

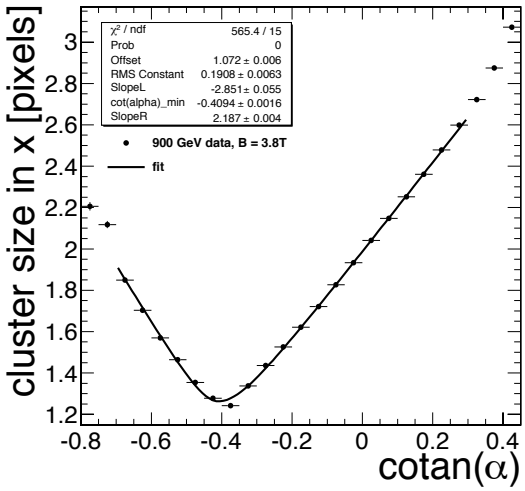

Figure 10.9: Cluster size as a function of incidence angle for minimum bias events. Solid lines represent fits to the data points.

placement was measured as a function of production depth from tracks with shallow impact angles (Fig. 10.8). The large number of low momentum tracks at 900 GeV also allowed a measurement using the cluster size technique (Fig. 10.9). In all cases excellent agreement was obtained with the results of a PIXELAV simulation (Table 10.1).

10.2 Spatial alignment of the silicon pixel and strip tracker

The alignment of the CMS tracker is a complex task in view of the very large number of silicon sensors (about 15'000) and their excellent position resolution. Two alignment algorithms are being used: the *Hit and Impact Point (HIP)* algorithms used by the Zurich groups, and the *Millepede* approach. While the latter is suitable to detect large movements, the former can lead to very precise positions for small distances. Hence the best alignment precision is obtained by applying the *HIP* algorithm starting on sensors positions previously obtained with the *Millepede* algorithm. We collected a large sample of cosmic ray tracks in summer 2009 before LHC operation. The data allowed a precise spatial alignment of the tracker after the hardware interventions of the previous year. The analysis of alignment data taken with pp-collisions is in progress. The alignment of the pixels can be achieved with a typical precision of 2 μm (4μm) in the transverse (longitudinal) directions.

Table 10.1: **Lorentz angle θ_L in the barrel pixel detector determined with two different techniques, using cosmic ray tracks and minimum bias events from LHC collisions.**

sample	method	$\tan\theta_L$ [a]	
		measurement	PIXELAV simulation
cosmic rays	cluster size	0.4071(20)	0.3972(30)
collisions	grazing angle	0.3985(5)	0.4006(5)
collisions	cluster size	0.4094(16)	0.4113(48)

[a] statistical error only

10.3 Improvements to the pixel hit reconstruction

Searches for the Higgs boson or new particles beyond the Standard Model (such as SUSY), depend heavily on the identification of τ-leptons and b-quark jets. For example, the τ-lepton decays into three charged pions (and an invisible neutrino) with a branching ratio of about 10%. Since the transverse momentum of the τ-jet is large compared to the τ mass, the decay pions emerge in a strongly collimated jet in which the charged tracks stay in close proximity. The larger the τ momentum, the more strongly collimated the three tracks, which makes them inseparable when the pixel hits merge into one large cluster. This occurs in the innermost pixel layer when the opening angle between the two trajectories is below 5 mr, which corresponds to a transverse momentum of 150 GeV/c for a typical 3-prong decay. This effect deteriorates the measurement of the particle trajectories and the reconstruction of the τ mass. Thus, an excellent spatial resolution is needed for τ reconstruction.

The measured cluster charge and track impact angles can be used to discriminate merged hits from isolated hits. Figure 10.10 shows a simulation of the pixel cluster charge distribution, corrected for the traversed path length, for merged and isolated clusters produced by τ decays. Merged clusters produce satellite peaks at twice or three times the minimum ionizing energy deposit and can therefore be recognized.

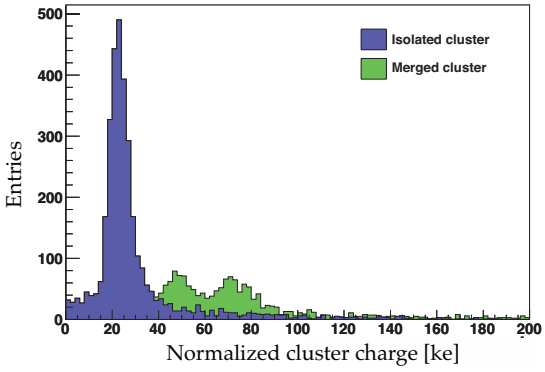

Figure 10.10: Pixel cluster charge distribution (corrected for impact angle) for hadronic τ decays. The blue histogram shows isolated clusters, while the green histogram shows the merged hits.

From simulations we have also shown that the splitting of merged clusters has an impact on the track parameter resolutions and on the b-jet selection efficiency. We are therefore implementing a cluster splitting technique in the pixel hit reconstruction software which we intend to use for Higgs searches in τ decays.

10.4 Improvements to b-quark tagging techniques

The b-tagging algorithms in the CMS fast Monte Carlo simulation (12) are under our responsibility. The fast b-tagging uses the same algorithms as the full detector simulation and reconstruction. The disadvantage is that the agreement between fast and full (GEANT4 based) detector simulations is not perfect in all regions of phase space. Various improvements have therefore been implemented:

- **pixel hit merging**
  Since the track reconstruction in the fast simulation does not include the step of pattern recognition, faked tracks are not reproduced. Thus, detector effects such as hit sharing between tracks or cluster merging (section 10.3), are not simulated. To estimate the contribution from these effects, a pixel hit merging algorithm was implemented in the fast simulation and tracks with shared hits were removed in the full detector reconstruction.

- **material effects**
  Particles traversing the tracking detectors are subject to multiple scattering, nuclear interactions and conversions (for photons).

The fast simulation uses a simplified detector geometry and the material budget is tuned according to the amount of photon conversions obtained from the full simulation. This simplified geometry potentially introduces biases which affect the tracking performance in the inner layers. These effects have been investigated by varying the thickness of materials.

- **pixel hit parameterization**
  The resolution of pixel hits was parameterized and tuned according to the full detector simulation.

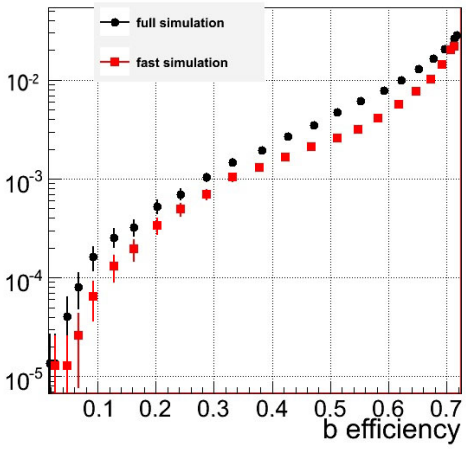

Figure 10.11:
Misidentification rate of the "secondary vertex" b-tagging algorithm vs. tagging efficiency, before the improvements described in the text.

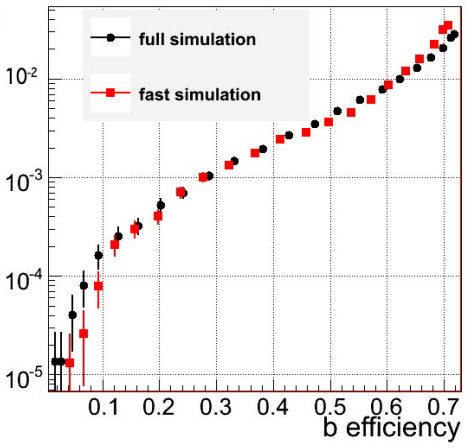

Figure 10.12:
As in Fig. 10.11 after the improvements.

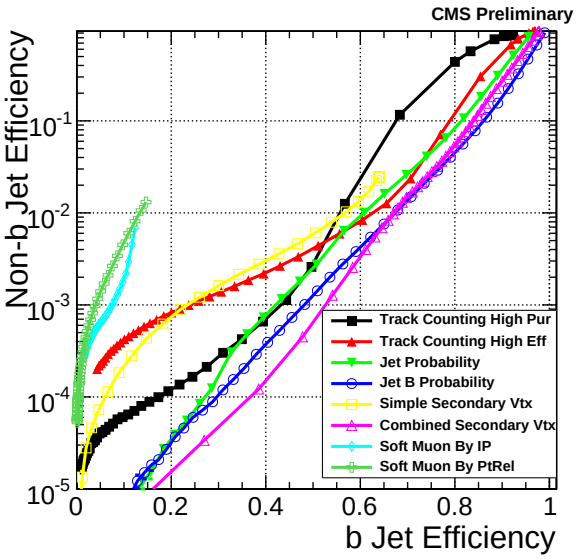

Figure 10.13: Mistagging efficiency of all CMS b-tagging techniques vs. b-tagging efficiency (from refs. [13; 14]).

Figures 10.11 and 10.12 display the performance of the secondary-vertex based b-tagging algorithm, without and with the new features, respectively. Depending on b-tagging efficiency, the misidentification rate increases by up to a factor of two, and agrees almost perfectly with the full simulation.

A comparison of the CMS b-tagging algorithms is shown in Fig. 10.13. During the 2010 runs we will monitor of the physics observables used in the b-tagging algorithms and determine the algorithm performances with data-driven methods.

10.5 Studies of $B_s \rightarrow (J/\psi)\phi$ and B_c-decays

The lifetime of the B-mesons is relatively long and the CMS pixel detector can determine B-decay vertices precisely. This reduces the background substantially and facilitates measurements of the B_s mass and mean life, and the measurement of B_s mixing parameters, such as the width

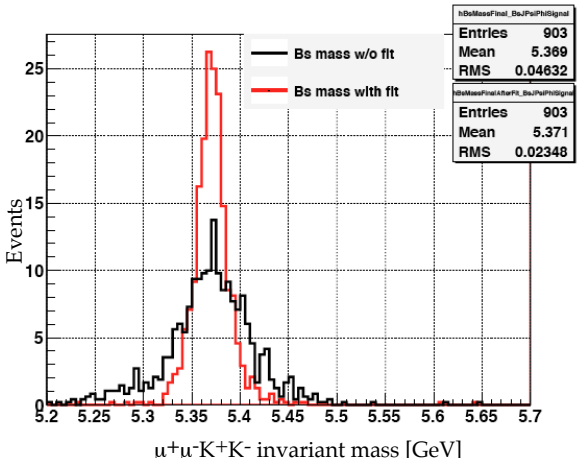

Figure 10.14: Mass distribution in the B_s region with and without kinematic fit (simulation).

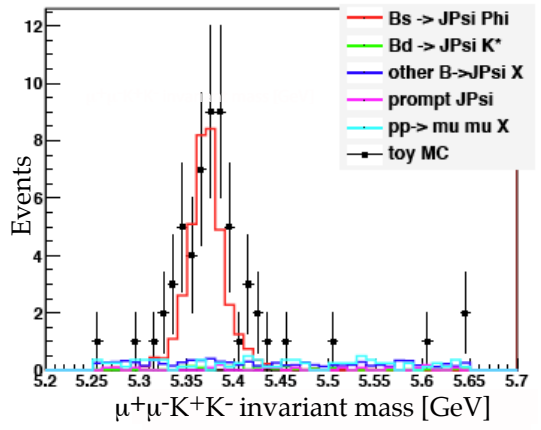

Figure 10.15: Reconstructed B_s-mass spectrum for 1pb^{-1} at 10 TeV.

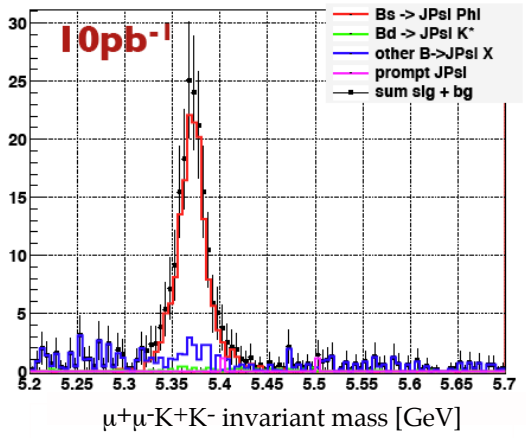

Figure 10.16:
Reconstructed B_s-mass spectrum for 10 pb^{-1}.

difference between the B_s^H andB_s^L mass eigenstates, together with the CP violating weak phase, which is sensitive to physics beyond the Standard Model.

Physics involving the b-quark will be among the first studies to be performed with LHC data. We have studied in detail the decay channel $B_s \to (J/\psi)\phi \to (\mu^+\mu^-)K^+K^-$ (9; 15). B_s-decays into J/ψ are selected during data taking using a di-muon trigger. Events are further selected offline by requiring two opposite sign muons from the J/ψ and a common vertex from the J/ψ and ϕ particles, and cutting on the transverse momentum of the kaons from ϕ decay. To reconstruct $B_s \to (J/\psi)\phi$ additional quality cuts are applied on the observables and a kinematic fit is applied. Figure 10.14 shows the factor of two improvement to the reconstructed B_s mass width obtained with the kinematic fit.

We will observe the $B_s \to (J/\psi)\phi$ decay already with an integrated luminosity of 1 pb^{-1}. We will then determine the B_s mass and mean life with 10 pb^{-1}, measure the CP-even and CP-odd components with more than 50 pb^{-1}, and extract the CP weak phase difference with more than 100 pb^{-1}. Figures 10.15 and 10.16 show the reconstructed B_s invariant mass for 1 pb^{-1} and 10 pb^{-1}, respectively (from two

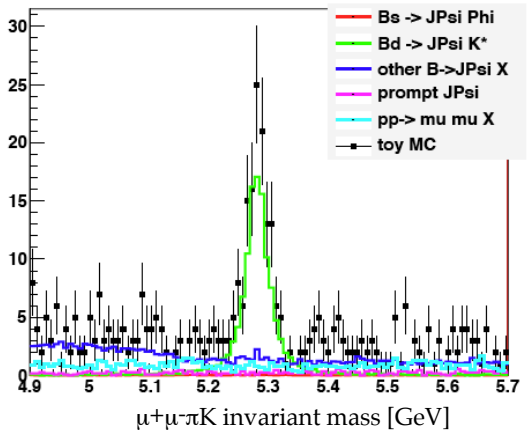

Figure 10.17:
Reconstructed B_d-mass spectrum for 1pb^{-1}.

analyses with slightly different cuts). The well measured channel $B_d \rightarrow (J/\psi)K^*$ was selected as calibration channel. Figure 10.17 shows the reconstructed B_d-mass using the same analysis code as for the B_s case shown in Fig. 10.16.

The B_c-meson is unique in that it is made of two different heavy quarks (b and c). We have started analyses to measure its mass and lifetime in two promising decay channels: $B_c^{\pm} \rightarrow J/\psi\ \rho^0\ \pi^{\pm}$ and $B_c^{\pm} \rightarrow J/\psi\ \rho^{\pm}$. The cleaner J/ψ-decay is into $\mu^+\mu^-$, but decays into e^+e^- pairs are also under investigation. In the first case, the ρ^0 decays into two charged pions, hence five tracks are associated to the same secondary vertex. In the latter case, the ρ^+ decays into a neutral and a charged pion, so three tracks and one electromagnetic cluster are produced.

10.6 Modeling of Higgs and jet production at the LHC

One of the main motivations for the LHC physics program is the study of the electroweak symmetry breaking mechanism and the Higgs boson discovery. The direct production of the Higgs boson via a top loop coupling to the incoming gluons has the largest cross-section, and hence is the most promising discovery channel, in particular via decays into two vector bosons. The survey of the different Higgs boson signatures above the Standard Model background will rely on data-driven studies, but also on comparison with Monte Carlo expectations.

For years, efforts have been made to develop Monte Carlo programs capable to model the collisions as accurately as possible, using both fixed order perturbative calculations and by merging matrix-element and parton-shower algorithms. Using the generators Herwig, HNNLO, Madgraph/Madevent, MC@NLO, POWHEG and Sherpa (16), one of us participated in the study of Higgs boson production via gluon-gluon fusion We have provided results using a jet merging technique (K_t-MLM) implemented in $Madgraph\ /\ MadEvent$. While a minimal set of parameters was chosen to be fixed for all simulations (parton densities, t-mass, center-of-mass energy), no detailed tuning was performed. The predictions from event generators for rapidity and transverse momentum of the Higgs boson are shown in Figs. 10.18 and 10.19, respectively (16).

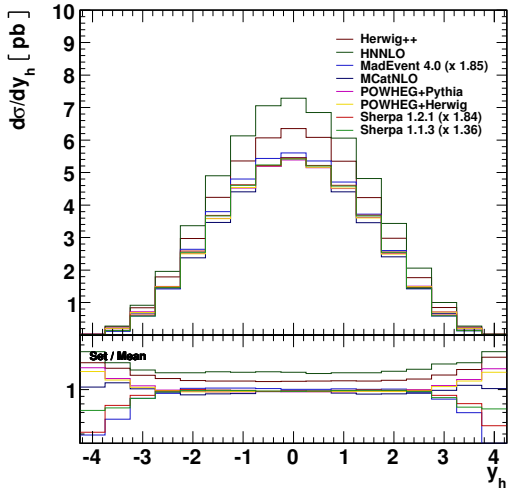

Figure 10.18: Rapidity distributions of the Higgs boson for LHC collisions predicted by different Monte Carlo simulations (from [16]).

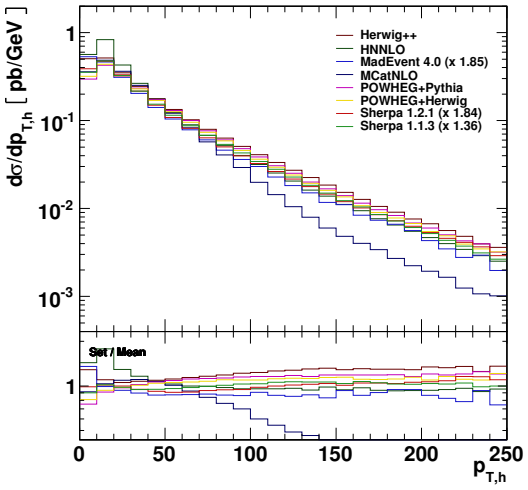

Figure 10.19: The corresponding transverse momentum distributions

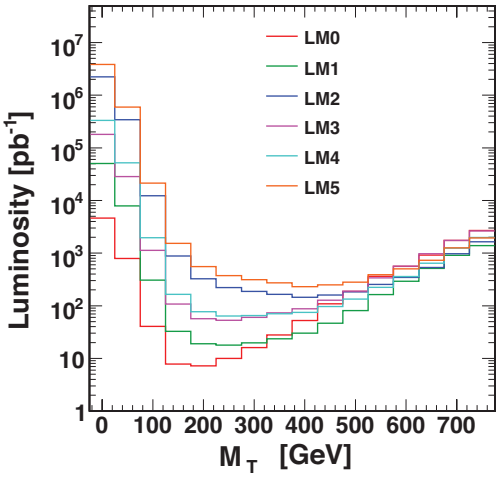

Figure 10.20: Integrated luminosity required for SUSY discovery as a function of cuts on M_T for various points of the mSUGRA parameter space[21].

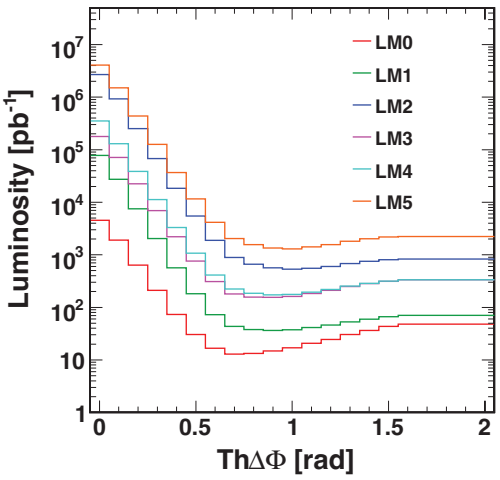

Figure 10.21: As for Fig. 10.20 but with cuts on $Th\Delta\Phi$.

10.7 Search for Supersymmetry (SUSY) in multi-jet final states

In previous annual reports we reported on SUSY decays into 2 jets, no missing lepton and large missing energy. In 2009 the Monte Carlo study of Supersymmetry in di-jet events (17) was refined and extended to higher jet multiplicities (18). Other approaches to reduce background have been studied and compared in terms of signal significance and robustness against systematic uncertainties. The basic selection for SUSY searches in hadronic final states relies on missing transverse energy. The corresponding cut is very effective in rejecting a large part of the QCD multi-jet background. Apart from the missing transverse energy M_T, another variable based on the global transverse thrust is useful, $Th\Delta\Phi$ (19): The direction of the thrust axis is used to combine all jets in an event into two pseudo-jets emitted into two hemispheres. The variable $Th\Delta\Phi$ is then the angle between the two pseudo-jets in the transverse plane.

Ignoring in a first step systematic uncertainties, the required minimum luminosity for a 5σ discovery of SUSY beyond Tevatron reach (20) is about 10 pb^{-1} (Figs. 10.20 and 10.21). Systematic errors are due to uncertainties in the jet energy scale and the azimuthal angle. They were studied in detail and found to lead to an increase of the required minimum luminosity by about a factor two to three, depending on whether the $Th\Delta\Phi$ or the M_T cut is used.

10.8 Upgrades of the computing infrastructure

We have assembled a computing cluster (TIER4) for our group at CERN, which is regularly upgraded. The computing cluster proved to be essential to achieve prompt physics results, a clear asset in the early phases of data analysis, when the data load will not be too heavy. In 2009 five additional blades were installed for a total of 20 (3.3 GHz) CPU cores. The storage capacity was expanded to 50 TB by adding a new 14 TB disk array. The network

was submitted to a major revision and the GB Ethernet switches were replaced with a 10 GB device. One additional 4 GB FiberChannel switch was installed. For the CMS data taking during 2010, new software releases based on Scientific Linux 5 (SLC5) will benefit from improved C++ compilers. The current SLC4 will be deprecated. All of our machines are in the proces of being updated to SLC5.

10.9 Preparation for future upgrades of the CMS pixel detector

As a consequence of the latest LHC schedule review, the replacement of the current pixel system was postponed to the years 2016/17. Major upgrades are foreseen for the detector layout with the addition of a fourth barrel layer and a third disk in both endcap sections. The material thickness will be reduced by up to a factor of two in the central tracking region, thanks to new readout electronics and the evaporative cooling technique. The 0.13 μm CMOS technology for the front-end chip in the innermost layers is currently under evaluation. This technology allows a reduction of the pixel cell size, with corresponding improvements to the position and track resolutions in dense jets.

We performed a preliminary Monte Carlo study of the expected detector performances. The resolution on the hit position was studied as a function of pseudorapidity and cluster size with a sample of simulated muons. The resolution of the four track parameters that are measured by the pixel detector, namely the angles θ and ϕ, and the transverse and longitudinal impact parameters d_0 and d_z was also studied. As expected, the precision of track reconstruction is dominated by multiple scattering at low momenta, reaching an asymptotic value of $\sim$10 μm, respectively $\sim$30 μm, on the two impact parameters at high momenta. Estimates of the detector occupancy and b-tagging performance will be performed on a sample of simulated collisions events, and various pixel cell sizes will be compared.

[1] S. Chatrchyan *et al.* (CMS Collaboration), Journal of Instrumentation **3** (2008) S08004

[2] Y. Allkofer *et al.*, Nucl. Instr. Meth. in Phys. Res. **A584** (2008) 25

[3] V. Chiochia *et al.*, Nucl. Instr. Meth. in Phys. Res. **A568** (2006) 51

[4] A. Schmidt *et al.*, Journal of Instrumentation **4** (2009) P05003

[5] S. Chatrchyan *et al.*, (CMS Collaboration), Journal of High Energy Physics **02** (2010) 041

[6] S. Chatrchyan *et al.* (CMS Collaboration) Journal of Instrumentation **5** (2010) T03007

[7] A. Dorokhov *et al.*, Nucl. Instrum. Meth. in Phys. Research **A530** (2004) 71

[8] A. Dorokhov *et al.*, Nucl. Instrum. Meth. in Phys. Research **A560** (2006) 112

[9] L. Wilke, PhD Thesis, University of Zurich (2009)

[10] M. Swartz, Nucl. Instrum. Meth. **A511** (2003) 88

[11] L. Wilke, V. Chiochia, T. Speer, CMS Note 2008/012

[12] A. Schmidt, IEEE Nuclear Science Symposium Conference Record **N37-4** (2008) 2795

[13] W. Adam *et al.*, CMS Analysis Note 2009/085 and CMS PAS BTV-09-001.

[14] A. Schmidt, Proc. of Science (EPS-HEP 2009) 439

[15] K. Prokofiev, PhD Thesis, University of Zurich (2005)

[16] J. M. Butterworth *et al.*, Summary Report from the Les Houches 2009 Workshop on TeV Colliders, prep. arXiv:1003.1643 (2010)

[17] T. Rommerskirchen *et al.*, CMS Note PAS SUS-08-005

[18] T. Rommerskirchen *et al.*, CMS Note PAS SUS-09-001

[19] M. Weber *et al.*, CMS Note PAS QCD-08-003 (2008)

[20] G.L. Bayatian *et al.* (CMS Collaboration), J. Phys. G: Nucl. Part. Phys. **34** (2007) 995

[21] T. Rommerskirchen, PhD Thesis (in preparation)